Theoretical and Practical Validation of Combined BEM/FEM Substrate Resistance Modeling

E. Schrik, P.M. Dewilde and N.P. van der Meijs
Delft University of Technology, DIMES, Circuits and Systems Group
Mekelweg 4, 2628 CD, Delft, The Netherlands
e-mail: eelco@cas.et.tudelft.nl

Abstract

In mixed-signal designs, substrate noise originating from the digital part can seriously influence the functionality of the analog part. As such, accurately modeling the properties of the substrate as a noise-propagator is becoming ever more important. A model can be obtained through the Finite Element Method (FEM) or the Boundary Element Method (BEM). The FEM performs a full 3D discretization of the substrate, which makes this method very accurate and flexible but also slow. The BEM only discretizes the contact areas on the boundary of the substrate, which makes it less flexible, but significantly faster. A combination between BEM and FEM can be efficient when we need flexibility and speed at the same time. This paper briefly describes the BEM and the FEM and their combination, but mainly concentrates on the theoretical validation of the combined method and the experimental verification through implementation in the SPACE layout to circuit extractor and comparison with commercial BEM and FEM tools.

1 Introduction

In present-day micro-electronic designs, there is a tendency to incorporate both analog and digital circuitry on one chip. In these so-called "mixed-signal" designs, substrate noise can have a significant impact on the functionality of the design. Substrate noise originates from a mechanism as schematically drawn in Figure 1. Because of the resistive nature of the substrate, the ground connection is not ideal, and the high-frequency switching activity of digital devices will cause noise-like potential fluctuations in the substrate, which may seriously affect the behaviour of any sensitive analog devices.

To predict any problems in circuit performance caused by substrate noise, there is an increasing need for accurate models that describe the noise-propagation behaviour of the substrate [1, 2, 3, 4, 5, 6, 7, 8, 9, 10]. Such models are usually obtained through either the Finite Element Method (FEM) as applied in e.g. [4] or the Boundary Element Method (BEM) as applied in e.g. [10]. The FEM performs a full 3D discretization of the substrate, and therefore it is very versatile and flexible, but it is usually also slow. The BEM, on the other hand, assumes the substrate to consist of uniform layers and it only discretizes the contact areas on the boundary of the substrate. Therefore it is less flexible, but it can be significantly faster.

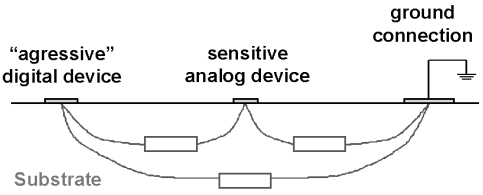

Figure 1: The substrate noise mechanism

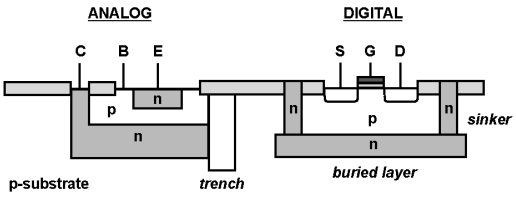

Figure 2: Doping patterns like trenches, buried layers, sinkers and channel-stoppers (not shown) may influence the noise characteristics of the substrate.

However, in some modeling problems, a dilemma arises when neither the BEM nor the FEM would be the most convenient method to use. Consider, for example, a substrate where the doping patterns (e.g. channel-stoppers, buried layers, sinkers and trenches as depicted in Figure 2) that are present in the top layers of the substrate are expected to have a significant influence on noise-propagation. While FEM-based modeling could accurately model such structures, it can often be too slow. On the other hand, the BEM might be significantly faster, but it may not be accurate enough, because the doping patterns do not form a uniform layer.

To circumvent this modeling dilemma, we have developed a combination of BEM and FEM [11] that is faster than FEM but can be more accurate than BEM based-methodologies. Our approach is to apply the FEM for the specific doping

0-7803-7607-2/02/$17.00 ©2002 IEEE

patterns, and the BEM for the underlying substrate, after which we combine the resulting models.

This paper introduces the combined BEM/FEM method and solidifies its theoretical and practical validity. Section 2 gives a brief background on the FEM and the BEM and their combination, followed by a convergence proof for the combined method in Section 3. Section 4 presents a few details on the implementation of the method into the SPACE layout-to-circuit extractor, and shows an application of our method, together with a successful comparison to commercial BEM and FEM tools. Finally Section 5 states our conclusions.

2 Background

In substrate resistance extraction, the aim is to find a resistance network between terminals placed on the boundary of a resistive (i.e. passive) domain. From physics, we know that resistance relates potential-differences to currents, which implies that we essentially need to solve a static potential-problem. From a mathematical point of view, this is equivalent to imposing (continuous) boundary conditions on the medium, and solving the Laplace equation

$$\nabla(\sigma\nabla\Phi) = 0 \tag{1}$$

where Φ is the potential-field and σ is the conductivity of the medium. A convenient property of the resulting field is that it has minimal energy according to the following energy functional

$$\mathcal{E}(\Phi(p)) = \int_{\Omega} \sigma||\nabla\Phi(p)||^2 dp \tag{2}$$

where Ω is the domain of interest and dp is the relevant volume integral. We can solve Φ with different methods.

Finite Element Method

The finite element method (FEM) subdivides the entire domain into triangular (2D) or tetrahedral (3D) elements (see Figure 3a), and treats the elements as linear. The mutual mathematical relations between the potentials at the corners of the elements (the FEM nodes) can then be expressed very easily by a piecewise linear (or piecewise planar for 3D) function. Through an incidence strategy which accumulates the FEM elements, a global system of mutual mathematical relations between the FEM nodes is obtained, which is then used to minimize the energy functional as described above. In this case, the energy functional is used as an alternative formulation of the Laplace equation. For an extensive analysis of the FEM, the reader is referred to [12].

However, if we take a slightly different approach to the FEM, the resistance network can be found without having to calculate the field solution. This approach is based on the observation that the mathematical relations along the edges in the FEM discretization already represent resistances (see e.g. [13]). In other words, the FEM discretization is equivalent to a resistance network. When this network is used for subsequent circuit simulation, the minimization of the energy functional will automatically (though implicitly) be ensured by the circuit simulator itself.

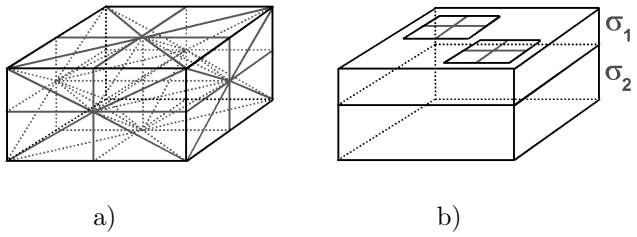

Figure 3: a) 3D tetrahedral FEM discretization; b) BEM discretization of contact areas on top of uniformly layered domain

The network that we find in this way has many nodes and a sparse structure. However, only a small number of the FEM nodes are actually terminal nodes, while the rest of the FEM nodes are internal nodes. Therefore, any internal nodes can be eliminated through Gaussian elimination, or, equivalently, star-delta transformation.

The 3D discretization will automatically incorporate any inhomogeneities of the domain into the model, because each element in the discretization can have its own material properties assigned. As such, the FEM is very accurate and flexible.

Boundary Element Method

The Boundary Element Method (BEM) is based on an integral form of the Laplace equation [10, 14]

$$\Phi(p) = \int_{S_1} k(q)G(p,q)dq \tag{3}$$

where $S_1 \subset S$ is the entire contact area on the boundary surface S, dq represents the relevant surface integral, $k(q)$ represents the unknown continuous current density, and, $G(p,q)$ is the Green's function. The Green's function is a fundamental solution to the Laplace equation, and, as such, it automatically ensures the minimization of the energy functional.

The Green's function "encodes" the characteristics of the medium, and it can be interpreted physically as "the potential in point p due to a current injected at point q". For the 3D homogeneous case, the Green's function is

$$G(p,q) = \frac{1}{4\pi\sigma r} \tag{4}$$

where $r = \sqrt{(p_x - q_x)^2 + (p_y - q_y)^2}$ (the p_z and q_z coordinates have deliberately been omitted, because the contact areas are situated on the top plane of the substrate). Also for uniform, layered media (see layers σ_1 and σ_2 in figure 3b) a Green's function can be determined, but it is not possible to include localized doping patterns as depicted in Figure 2.

The BEM only has to discretize those parts on the boundary of the domain (see Figure 3b) where Dirichlet conditions hold (i.e. the contact area S_1 where current can enter / leave the domain), and assumes the remaining part of the boundary

to be subject to Neumann conditions. Similar to the characteristics of the medium, these boundary conditions can also be "encoded" by the Green's function.

The discretization usually (but not necessarily) utilizes rectangular panels and assumes the current distribution to be constant on each panel (i.e. each panel forms an equipotential region). As such, the discretization allows a piecewise constant approximation of the continuous current density distribution. Based on the discretization, the Method of Moments [15] allows us (either through the collocation method or the Galerkin method) to find this approximation from a linear system of equations. In this case, we define $\mathbf{P}$ as the vector of panel potentials, $\mathbf{K}$ as the vector of (unknown) panel currents and G as the elastance matrix describing the potential at panel i due to a unit current in panel j (i.e. the Green's function is evaluated for each panel-pair)

$$\mathbf{P} = G\mathbf{K} \tag{5}$$

The BEM then continues by defining an incidence matrix F relating panels and contacts. By denoting $\mathbf{V}$ as the contact potential vector and $\mathbf{I}$ as the contact current vector, we can write

$$\mathbf{P} = F\mathbf{V} \tag{6}$$

$$\mathbf{I} = F^T\mathbf{K} \tag{7}$$

It follows that

$$\mathbf{I} = F^T G^{-1} F\mathbf{V} = Y\mathbf{V} \tag{8}$$

where Y is an admittance matrix for the resistive substrate with the substrate contacts as ports.

Thus, we see that also with the BEM the result is a resistance network. Compared to the FEM, however, this is a *full* resistance network, where each node is a port-node that is connected to every other node; there are no internal nodes. Model order reduction should be used to simplify this network, and/or a windowing technique such as [10] can be used to a-priori extract a reduced order model.

Combining FEM and BEM

When making use of dedicated, highly optimized solution methods for both BEM and FEM, the BEM is usually significantly faster, but this is typically at the expense of flexibility. Therefore, as already mentioned in the introduction, some substrate modeling problems pose a dilemma when neither the BEM nor the FEM would be the most convenient method to use. In such a case, we can supply the BEM with some of the flexibility of the FEM, by applying the FEM to the specific doping patterns (recall Figure 2), and the BEM for the underlying substrate [11]. In effect, the BEM and the FEM are then confined to their own domains and communicate through an interface. Because both the BEM and the FEM result in resistance networks, the methods can be combined by properly aligning the nodes along the interface, after which the networks can be attached at the coinciding nodes. This requirement can be met by conveniently choosing the BEM mesh with respect to the FEM mesh.

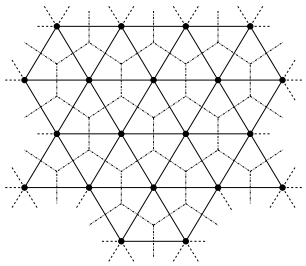

Figure 4: Dual meshing: the hexagonal BEM mesh is the dual of the triangular FEM mesh

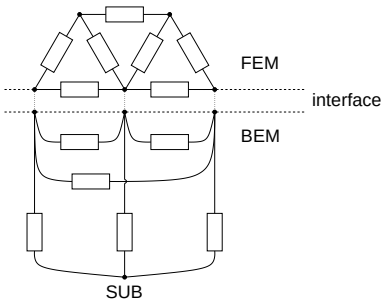

Figure 5: Side-view of the FEM and BEM areas together with the structure of the resulting resistance models. Due to dual meshing, the nodes on the interface will coincide, and a direct connection between the models can be made.

Basically, we want to achieve that a BEM panel be associated with every FEM node on the interface. This requirement suggests a dual relationship between the BEM and FEM meshes. Different interpretations of "duality" are possible, but the triangular interface mesh of the FEM reminds us of the duality between the Delaunay triangulation and the Voronoi tesselation. Even though the FEM mesh may not necessarily be a *true* Delaunay triangulation, choosing the BEM mesh as the Voronoi tesselation of the FEM nodes will still ensure a one-to-one association between the FEM nodes and the BEM panels (see Figure 4). Near the interface, the resulting networks will then look as illustrated in Figure 5.

An alternative way of combining the methods for capacitance extraction was presented in [16] where the BEM and FEM meshes coincided. In this case the interface nodes did not align and generalized ideal transformers were necessary for proper interaction between both models and for conservation of energy along the interface. This combination method was proven to converge in [17].

Below, we will give a similar, but slightly different proof of our method.

3 Proof

The key behind the proof is the fact that a field (Φ_m) that satisfies the Laplace equation and that satisfies the contin-

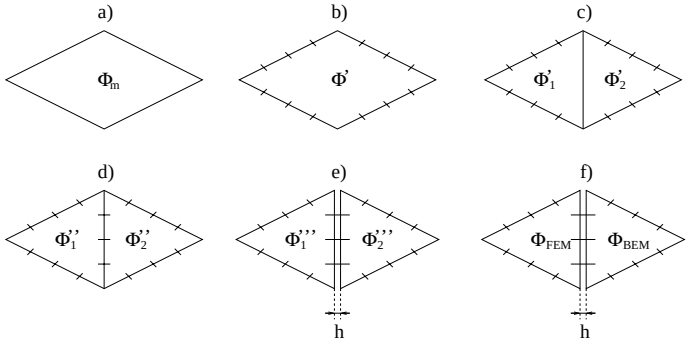

Figure 6: Different stages in the convergence proof

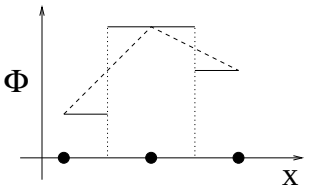

Figure 7: Field phenomena at the interface. The dots along the x-axis represent the coinciding BEM and FEM nodes. Legend: solid line = BEM boundary field, dashed line = FEM boundary field

uous boundary conditions imposed on the domain will have minimum energy (illustrated in Figure 6a). This is indeed the true, physical field. Additionally, we observe that fields that approximately satisfy the boundary conditions and whose energy lies close to the minimum are actually close to the exact field as well.

When the boundary conditions are discretized (illustrated in Figure 6b), the field will alter itself to a new field (Φ') such that its energy is minimal, consistent with the discretized boundary. By making the discretization fine enough, the approximate field Φ' can get arbitrarily close to the exact field Φ_m. In other words $\mathcal{E}(\Phi')$ can get ε-close to $\mathcal{E}(\Phi_m)$

We now divide the domain with an interface (Figure 6c). If the interface preserves energy (i.e. $\mathcal{E}(\text{interface}) = 0$), there will be an exact and continuous match between fields Φ'_1 and Φ'_2 along the interface, such that the total field will have minimal energy, and will be consistent with the discretized boundary conditions along the outer boundary.

When discretizing this interface (Figure 6d), there will be an exact, but *discrete* match between Φ''_1 and Φ''_2 along the interface, such that the total field is still consistent with the conditions on the outer boundary. However, because the discretized potential distribution on the interface *approximates* the *exact* distribution, we know that the total field may not have minimal energy.

In our combined BEM/FEM method, the "discrete match" between Φ_{BEM} and Φ_{FEM} (see Figure 7) is performed by attaching the coinciding interface nodes. However, discretization of the interface also introduces an anomaly in the field, because of field discontinuities along the interface, halfway between the coinciding nodes (see Figure 7). Assuming a solution to the field problem for the BEM/FEM discretized case, which also matches in a discrete way on the internal interface, we will now study the energy contained within the anomaly. Therefore, we introduce an h-thin layer along the interface, by which we effectively separate the domains to which the fields belong (Figure 6e).

As illustrated in Figure 6f, there is a FEM field on the left and a BEM field on the right of the interface. Figure 7 shows both fields. A difference field will now exist across the h-thin layer. This field is defined by taking Φ_{BEM} and Φ_{FEM} in point x on the interface, and do a linear interpolation across the distance h:

$$\Phi_i(k,x) = \Phi_{FEM}(x) + \frac{\Phi_{BEM}(x) - \Phi_{FEM}(x)}{h} \cdot k \cdot h \qquad (9)$$

Here, Φ_i stands for the potential inside the h-thin layer; k and x, are such that k is contained within the continuous interval $[0,1]$ and x is the relevant point on the interface. The result is a piecewise continuous field.

We observe that the mesh granularities of the BEM and the FEM meshes should be proportional to the thickness of the h-thin layer. In this way, the derivative of the linear interpolation will be kept in proportion while $h \to 0$.

As shown in Figure 7, Φ_{BEM} is piecewise constant. Thus, for a mesh granularity of "h", we know, through a Taylor expansion, that in a given point p, Φ_{BEM} is $O(h)$ away from the exact field for the situation of Figure 6e. Similarly, since Φ_{FEM} is piecewise linear, we know that in the same point p, Φ_{FEM} is $O(h^2)$ away from the exact field.

In terms of energy, we need the derivative of Φ_i. From Equation (9), we find this to be:

$$\nabla\Phi_i = \frac{\Phi_i|_{k=1} - \Phi_i|_{k=0}}{h} = \frac{\Phi_{BEM} - \Phi_{FEM}}{h} = \frac{O(h)}{h} = O(1) \qquad (10)$$

Because the h-thin layer has constant thickness h, we can rewrite the energy integral as follows:

$$\int_{V_i} ||\nabla\Phi_i||^2 dv \quad \Longrightarrow \quad \int_{S_i} ||\nabla\Phi_i||^2 \, h \, dS \qquad (11)$$

where V_i is the volume of the h-thin interface layer and S_i is the surface of the interface layer. We finally prove the $O(h)$ convergence with

$$\lim_{h\to 0} \int_{S_i} O(1) \, h \, dS = 0 \qquad (12)$$

We have now seen that the energy contained within the anomaly in the interface field, disappears as $O(h)$. We observe that the "total field" formed by combining the two fields with their linear interpolation is continuous and piecewise differentiable. Thus, the total field belongs to the same "search-space" as Φ_m and Φ'. Additionally, we observe that the total field minimizes energy, because both the BEM and the FEM minimize energy (see Section 2), and the interface contributes a negligible portion to the total energy.

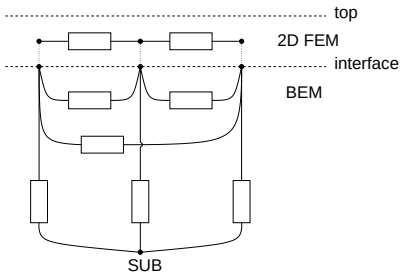

Figure 8: Side-view of the 2D FEM and the BEM models, under dual meshing (compare Figure 5)

Summarizing, the situation is as follows: (1) The energy of the field obtained in Figure 6d may not be minimal, because the discretized potential distribution on the interface differs from the exact distribution. Nevertheless, the energy is ε-close to the exact field in 6c; (2) The field in 6f has energy necessarily smaller than that of 6d because BEM and FEM minimize the energy and the mismatch in the interface contributes a negligible part to the total energy; (3) The minimum obtained in 6f goes over a search-space that is part of the search-space for 6c. Hence, all these fields are ε-close to each other in energy and hence in point-values. This concludes the principle of our proof.

4 Experiments

We have implemented a first prototype of our method into the SPACE layout-to-circuit extractor [18]. The prototype (see Figure 8) utilizes a 2D FEM instead of a 3D FEM for the specific doping patterns and a BEM for the underlying substrate. The 2D FEM is a valid modeling methodology, as long as the FEM domain is thin and has a significantly lower resistivity than the BEM domain.

Additionally, because calculating the BEM for hexagonal panels (recall Figure 4) is computationally less efficient, our prototype does not use dual meshing, but constructs independent BEM and FEM meshes and combines the networks based on proximity of the FEM nodes and the centers of gravity of the BEM panels. In other words, each (rectangular) BEM panel is now associated with the nearest FEM node.

An experimental verification of the convergence of our method was already done in [11]. With the following experiment, we will demonstrate the behaviour of our method in a more practical context.

In mixed signal designs, guard rings are sometimes used to improve the noise isolation between the digital and the analog part of the chip. This experiment will show how our model behaves for such structures, but note that it is specifically not intended as a design optimization or as an evaluation of guard-ring effectivity; it is only intended as an illustration of a possible application of our method.

The basic setup of this experiment is shown in Figure 9. It represents two terminals A and B that both have size $2\mu m \times 2\mu m$ and that are $30\mu m$ apart (center to center). Terminal B is surrounded by a guard ring that is grounded at terminal G. The parameter d controls the size of the guard ring while keeping it square.

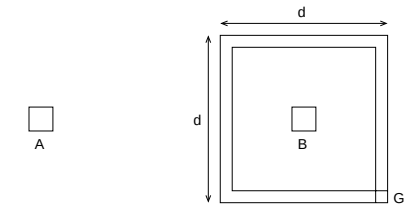

Figure 9: Basic guard-ring structure

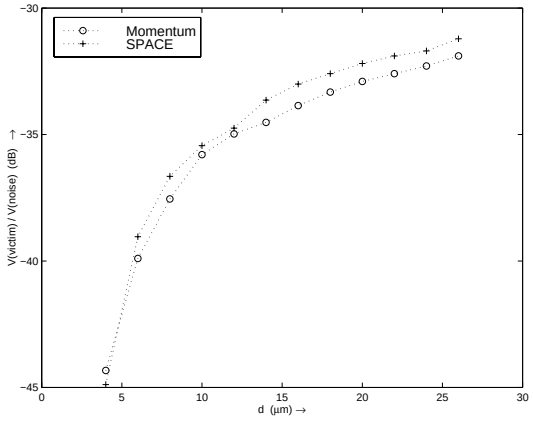

Figure 10: Sensitivity (in dB) of the noise victim as a function of guard-ring size.

The prototype implementation is such that the 2D FEM *only* discretizes the guard ring. The BEM wil now see Terminal A and Terminal B as "single" substrate contacts, and the guard ring as a "lumped" contact.

The substrate has a uniform resistivity of 10 S/m, and a backplane metallization. The guard ring has a resistivity of 1000 Ω/sq, a width of 1 μm and a thickness of 0.5 μm.

We calculate the sensitivity of the victim terminal (i.e. terminal B) with respect to the noise terminal (i.e. terminal A) through the following expression:

$$S[dB] = 20 \log \left(\frac{V_{victim}}{V_{noise}} \right) \tag{13}$$

Figure 10 shows the results generated with both SPACE and Momentum [19]. We clearly see that the results are very close to each other, and that the shape of the curve is intuitively correct.

Our method places the FEM domain *on top* of the substrate, whereas the FEM domain should actually be *embedded in* the substrate. Therefore, we have to determine how good our method is as an approximation of the actual situation. We have done that by comparing our results to those of the 3D FEM device simulator Davinci [20].

The basic layout is shown in Figure 11. It is a similar setup

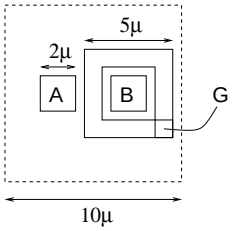

Figure 11: Guard-ring structure with reduced size

Table 1: Resistances (in $k\Omega$), Sensitivity and extraction time for the guard-ring structure

	R_{AB}	R_{AG}	R_{BG}	S(dB)	time(s)
SPACE	150	29.1	21.8	-17.9	28
Davinci	187	33.0	19.8	-20.4	325

as in Figure 9, but it has a drastically reduced size because of the limitations involved with Davinci being a device simulator. The substrate has a conductivity of 10 S/m and is $5\mu m$ thick, but without backplane metallization. The guard ring has a conductivity of 1000 S/m, is 1 μm wide and is 0.5 μm thick. For Davinci, we have assumed an n-type silicon substrate with doping concentration $N_d = 4.6 \cdot 10^{14} cm^{-3}$ and an n-type guard ring with $N_d = 4.6 \cdot 10^{16} cm^{-3}$, which correspond to 10 S/m and 1000 S/m, respectively.

The results can be found in Table 1, which was obtained using suitable mesh settings such that the results from both methods had converged (Davinci used 26011 grid points, where a maximum of 30000 was allowed for this version of Davinci). The table clearly shows that the results of the FEM method and the FEM/BEM method are reasonably close. There can be many reasons for the remaining differences, including the fundamental fact that the FEM (Davinci) needs a bounded domain (a cuboid) and the BEM (SPACE) assumes a domain laterally extending to infinity. The table also shows that our method can be considerably faster.

5 Conclusions

This paper describes a theoretical analysis and a practical application of a combined BEM / FEM method for substrate resistance modeling. Combined BEM/FEM modeling may be efficient in cases where accuracy as well as speed are required, but where a separate BEM would not be accurate enough and a separate FEM would not be fast enough.

In our theoretical analysis, we have proven that our combined BEM/FEM method converges linearly ($O(h)$) with the discretization at the BEM/FEM interface. As a practical application, we have used our method to model the substrate-resistances and the noise-sensitivity in a simple guard-ring structure. Our results were confirmed by two commercially available tools: Momentum [19] and Davinci [20].

Our future research will concentrate on schemes for simultaneous solution of BEM/FEM models and on model reduction.

References

[1] R. Gharpurey and R.G. Meyer, "Modeling and Analysis of Substrate Coupling in Integrated Circuits," *IEEE Journal of Solid-State Circuits*, vol. 31, pp. 344–353, Mar. 1996.

[2] N.K. Verghese, T. Schmerbeck, and D.J. Allstot, *Simulation techniques and solutions for mixed-signal coupling in ICs*. Boston: Kluwer Academic Publishers, 1995.

[3] R. Singh, "A Review of Substrate Coupling Issues and Modeling Strategies," in *Proc. CICC*, pp. 491–498, May 1999.

[4] F.J.R. Clement, E. Zysman, M. Kayal, and M. Declercq, "LAYIN: Toward a global solution for parasitic coupling modeling and visualization," in *Proc. IEEE Custom Integrated Circuits Conference*, pp. 537 – 540, May 1994.

[5] K.J. Kerns, I.L. Wemple, and A.T. Yang, "Stable and Efficient Reduction of Substrate Model Networks Using Congruence Transforms," in *Proceedings DAC*, pp. 207 – 214, 1995.

[6] X. Aragones, J.L. Gonzalez, and A. Rubio, *Analysis and Solutions for Switching Noise Coupling in Mixed-Signal ICs*. Boston: Kluwer Academic Publishers, 1999.

[7] P. Miliozzi, L. Carloni, E. Charbon, and A. Sangiovanni-Vincentelli, "SubWave: a Methodology for Modeling Digital Substrate Noise in Mixed-Signal IC's," in *Proceedings IEEE CICC*, pp. 385 – 388, 1996.

[8] M. Pfost, H.M. Rein, and T. Holzwarth, "Modeling Substrate Effects in the Design of High-Speed Si-Bipolar IC's," *IEEE Journal on Solid-State Circuits*, vol. 31, pp. 1493 – 1501, Oct. 1996.

[9] D.K. Su, M.J. Loinaz, S. Masui, and B.A. Wooley, "Experimental Results and Modeling Techniques for Substrate Noise in Mixed-Signal Integrated Circuits," *IEEE Journal of Solid-State Electronics*, vol. 28, pp. 420–430, Apr. 1993.

[10] T. Smedes, N. P. van der Meijs, and A. J. van Genderen, "Extraction of Circuit Models for Substrate Cross-talk," in *Proc. Int. Conf. on Computer-Aided Design*, (San Jose, California), pp. 199–206, Nov. 1995.

[11] E. Schrik and N.P. van der Meijs, "Combined BEM/FEM Substrate Resistance Modeling," in *Proceedings DAC 2002*, (New Orleans, LA), pp. 771 – 776, June 2002.

[12] G. Strang and G.J. Fix, *An Analysis of the Finite Element Method*. Englewood Cliffs: Prentice-Hall, Inc., 1973.

[13] J.E. Hall, D.E. Hocevar, P. Yang, and M.M. McGraw, "SPIDER - A CAD System for Modeling VLSI Metallization Patterns," *IEEE Transactions on CAD*, vol. 6, pp. 1023 – 1031, Nov. 1987.

[14] C.A. Brebbia, *The Boundary Element Method for Engineers*. Plymouth: Pentech Press, 1978.

[15] R.F. Harrington, *Field Computation by Moment Methods*. New York: The Macmillan Company, 1968.

[16] E. B. Nowacka and N. P. van der Meijs, "The Hybrid Element Method for Capacitance Extraction in a VLSI Layout Verification System," in *Software for Electrical Engineering Analysis and Design (Proc. ELECTROSOFT '96)* (P.P. Silvester, ed.), (Pisa, Italy), pp. 125–134, Computational Mechanics Publications, May 1996.

[17] E. B. Nowacka, P. Dewilde, and T. Smedes, "A Hybrid Element Method for Calculation of Capacitances from the Layout of Integrated Circuits," in *Boundary Element Technology XI (Proc BETECH 96)* (R. C. Ertekin, C. A. Brebbia, M. Tanak, and R. Shaw, eds.), (Hawai, U.S.A.), pp. 415–425, Computational Mechanics Publications, May 1996.

[18] F. Beeftink, A.J. van Genderen, N.P. van der Meijs, and J. Poltz, "Deep-Submicron ULSI Parasitics Extraction Using Space," in *Design, Automation and Test in Europe Conference 1998, Designer Track*, pp. 81–86, Feb. 1998.

[19] *Momentum, a 2.5 D EM Simulator by Agilent EEsof, see http://eesof.tm.agilent.com.*

[20] *Davinci (Taurus), a 3D Device simulator by Synopsys, see http://www.synopsys.com.*